Power Mapping Studies on the Coil Connection of an Interior and Embedded Permanent Magnet Double Stator Generator

Article *in* Progress In Electromagnetics Research M · January 2024

DOI: 10.2528/PIERM23091404

6 authors, including:

M. Norhisam
Universiti Putra Malaysia
134 PUBLICATIONS **1,297** CITATIONS

SEE PROFILE

Hairul Faizi Hairulnizam
Universiti Putra Malaysia
1 PUBLICATION **0** CITATIONS

SEE PROFILE

(Received 14 September 2023, Accepted 29 December 2023, Scheduled 5 March 2024)

Power Mapping Studies on the Coil Connection of an Interior and Embedded Permanent Magnet Double Stator Generator

Nur Amira Ibrahim[1, *], Norhisam Misron[1, 2, 3, *], Hairul Faizi Hairulnizam[1], Chockalingam Aravind Vaithilingam[4], Nashiren Farzilah Mailah[1], and Ishak Aris[1]

[1] *Faculty of Engineering, Universiti Putra Malaysia, Serdang, Selangor 43400, Malaysia*
[2] *Institute of Nanoscience and Nanotechnology, Universiti Putra Malaysia, Serdang, Selangor 43400, Malaysia*
[3] *Institute of Plantation Studies, Universiti Putra Malaysia, Serdang, Selangor 43400, Malaysia*
[4] *Clean Technology Impact Lab, Taylor's University, Subang Jaya, Selangor 47500, Malaysia*

ABSTRACT: The increased electrical demand in electrical machines promotes the improvement in power density in double stator systems. The power mapping performance and density of a novel type of interior embedded permanent magnet for a double-stator generator (IEDSG) is investigated in this work. This study investigates the basic attributes of the proposed IEDSG by analyzing various load resistances and changing rotor speeds. The Finite Element Method (FEM) is used to model the generation capabilities that consider electromagnetic properties such as flux density and flux lines. The proposed IEDSG is then manufactured and tested in a laboratory environment to assess how effectively it will perform when being paired with a load circuit. The efficiencies of two unique coil connections — series coil and independent coil — are evaluated and compared. According to the experimental results, when operating at an 800-rpm rotating speed, the independent-coil connection delivers a peak power output of 1688 W, a 16% improvement over the series-coil connection.

1. INTRODUCTION

Businesses and academic institutions have shown a strong interest in the study of electrical power generation from renewable energy sources. To generate electrical energy, a prime mover and a generator are typically used in tandem. The shaft of the generator rotates due to an external force supplied by mechanical energy. Car engines, steam turbines, gas turbines, hydro turbines, and wind turbines are examples of primary movers. Permanent magnet synchronous machines have been utilized as generators due to their numerous advantages, including their quick response, high efficiency [1–3], and robust and economical mechanical structure.

The permanent magnet properties, structure, and losses influence the size and performance of a permanent magnet generator [4]. Furthermore, the available power of Permanent Magnet Generator (PMG) machines is affected by both voltage and inductance [5]. As a result, the number of poles and other features must be carefully chosen to achieve the desired inductance.

Many researchers have proposed structural alterations such as single stator for surface and interior permanent magnets [6, 7], double stator [11–16], and double rotor [17, 18]. Gieras et al. [6] observed that a surface permanent magnet with a single stator generator had a low inductance value, resulting in a narrow field weakening range and a low torque-generating current. Surface permanent magnets provide only electromagnetic torque, whereas interior permanent magnets can produce both electromagnetic and reluctance torque.

Following the magnetic flux path, surface permanent magnet machines are unaffected by reluctance variations caused by mounting the permanent magnet on a surface of the rotor core made of a magnetic material with generally consistent characteristics. This architecture eliminates the requirement for purposeful changes in magnetic saliency. Because of this, an interior permanent magnet may generate higher torque than a surface permanent magnet [8]. The integration of permanent magnets within the rotor distinguishes the interior permanent magnet from the surface permanent magnet. This integration results in an extremely high power density as well as a torque-to-inertia ratio [19, 20].

According to Pellegrino et al. [9], regardless of the current overload, the output power of the surface permanent magnet single stator generator cannot reach the continuous power rating, whereas the interior permanent magnet single stator generator has excellent overload capability across the entire speed range as the machine's salience increases. According to Yu et al. [10], even though surface permanent magnets are significantly easier to make because they are adhesively attached to the rotor surface, this may result in permanent magnets flying off. An interior permanent magnet will provide better durability because it is in the center of the rotor.

Chai et al. [11] developed a double-stator starter generator for hybrid autos in 2005 to improve performance per volume and performance cost ratio. Chau et al. built and analyzed a new double-salient permanent magnet machine with a flux-controlling outer rotor in 2006 [12]. Misron et al. [16] created a single-phase permanent magnet generator to achieve high output power and efficiency; the best configurations were es-

* Corresponding authors: Norhisam Misron (norhisam@upm.edu.my); Nur Amira Ibrahim (nuraamiraibrahim@gmail.com).

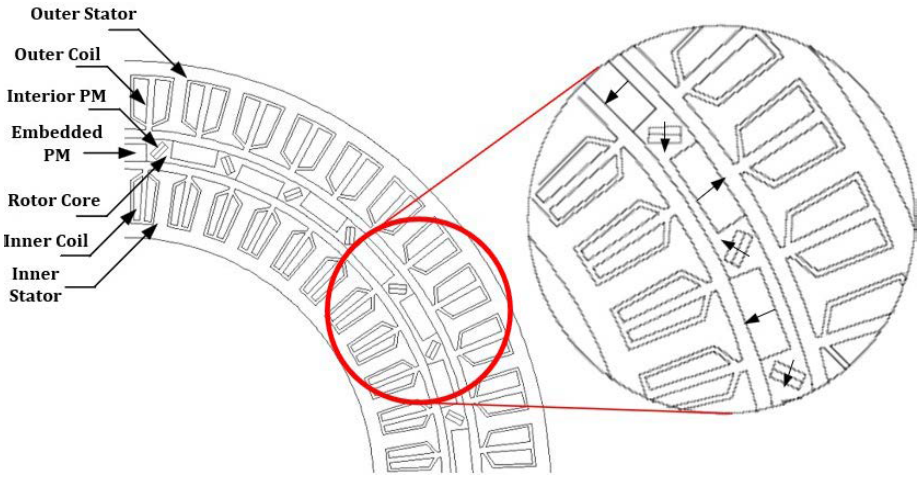

FIGURE 1. Structure of IEDSG.

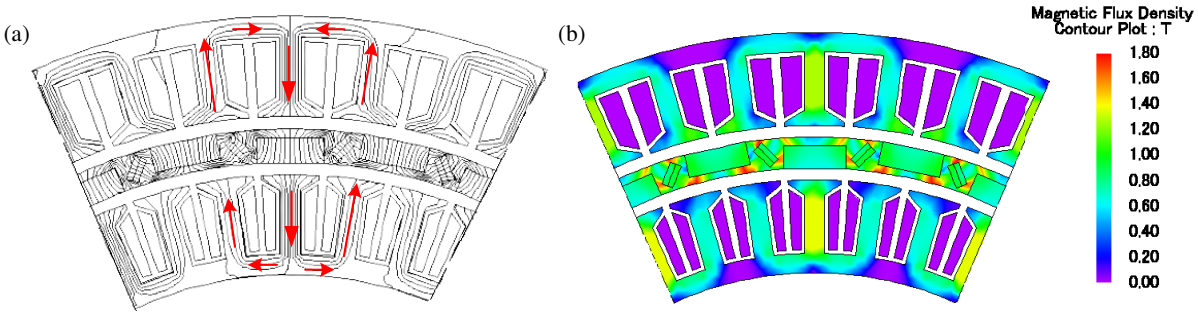

FIGURE 2. Magnetic flux distributions. (a) Flux lines. (b) Flux density.

tablished by altering the slot pole combination and length of the generator's outer stator yoke. The excellent flux linkage use of this double-stator topology results in high power density [16, 21, 22].

To increase the generator's power density, a double stator generator with an interior and embedded permanent magnet is suggested. The flux of the embedded permanent magnet will be forced through the air gap by the flux of the interior permanent magnet without returning to the permanent magnet itself. The performance features of the suggested machine are analyzed using a two-dimensional finite element technique (2D-FEM) numerical tool since it takes less time to simulate and has an accuracy difference of less than 10% compared to the three-dimensional finite element method. The power mapping method is used to analyze the performance of the coil connection under each condition's varied load and variable speed. The coil connection's performance is analyzed, and it is discovered that an independent coil provides 16% more power than a series coil connection.

2. IEDSG'S STRUCTURE AND WORKING PRINCIPLE

2.1. Structural Configuration

The suggested generator is made up of two stationary sections, the inner and outer stators, and one rotating part, which includes interior permanent magnet, embedded permanent magnet, and rotor core. To maximize flux connections and increase power density, the double stator generator was initially developed with a surface permanent magnet. However, the original design had a weakness that could result in large eddy current losses. As illustrated in Figure 1, this study presentes an interior and embedded permanent magnet for a double stator generator. Song et al. [23] investigated various rotor structures utilizing the finite element approach in conjunction with an optimal design procedure, commonly known as an iterative process, and concluded that this combination method has the maximum accuracy. As a result, the permanent magnets are available in two sizes based on an optimal design algorithm: 16 mm × 6 mm and 6 mm × 3 mm, commonly known as embedded PM and interior PM. An interior PM is a permanent magnet that has been inserted into the rotor core so that both of its surfaces are facing the rotor core. An embedded PM is a permanent magnet with one surface facing the rotor core and the other facing the inner or outer air gap.

The FEM simulation demonstrated the flux created by the interior and embedded PM utilized by both the outer and inner stators. The interior PM can increase the flux linkage from the embedded PM to the inner stator, making it easier for the flux to flow through the coil. The magnetic flux distributions in Figure 2 demonstrated that this is a radial flow, since the flux then proceeds down the stator, passing through the embedded PM and the air gap before entering the inner stator. The stator will get the most flux due to the force of the flux from the

inner PM, which will then flow to the outside air gap and give the most power. As shown by the flux density distributions and flux lines in Figure 2, the flux is distributed along the stator and permanent magnet, maximizing the usage of flux. Table 1 displays the proposed IEDSG specification.

TABLE 1. Specifications of proposed IEDSG.

Parameter	Value
Number of Poles	30
Number of Slots	45
Inner Diameter [mm]	175
Outer Diameter [mm]	300
Size of Interior PM [mm]	6×3
Size of Embedded PM [mm]	16×6
Outer and Inner Airgap [mm]	3

2.2. Working Principle

2.2.1. Series-Coil Connection

The series-coil connection and independent-coil connection are two ways that the IEDSG can be used. For the series-coil connection, the inner stator coil and outer stator coil are linked in series for each phase. As a result, the voltage generated at the inner and outer stators is what drives an IEDSG to produce electricity when the coil is connected in series. Equation (1) is used to calculate the produced voltage for a series connection.

$$E_{G_{series}} = 4.44f\left(N_{inner} + N_{outer}\right)\phi_{series} \ \text{[V]} \quad (1)$$

where $E_{G_{series}}$ represents the generated rms voltage in [V], f the frequency of the generator in [Hz], N_{inner} the number of inner coil turns, N_{outer} the number of outer coil turns, and ϕ_{series} the flux linkage through the series coil winding in [Wb]. The flow of the current at the series coil connection is calculated using Equation (2).

$$I_{a_{series}} = \frac{E_{G_{series}}}{\sqrt{\left(R_{series} + R_L\right)^2 + \left(2\pi f L_{series}\right)^2}} \ \text{[A]} \quad (2)$$

where $I_{a_{series}}$ represents the series current, R_{series} the series armature resistance of the coil winding, R_L the load resistance, and L_{series} the coil inductance. The total machine loss of an IEDSG is given by:

$$P_{l_{series}} = I^2_{a_{series}} R_{series} + \varepsilon_h f B^a + \varepsilon_e f^2 B^2 \ \text{[W]} \quad (3)$$

where $P_{l_{series}}$ is the total series losses power, ε_h the hysteresis coefficient, ε_e the eddy current coefficient, α a constant, and B the flux density of the magnet. The total series output power P_{series} generated is calculated based on Equations (4) and (5).

$$P_{series} = \left(E_{G_{series}}\right) I_{a_{series}} - P_{series\ losses} \ \text{[W]} \quad (4)$$

$$P_{series} = \frac{E^2_{G_{series}}}{\sqrt{\left(R_{series} + R_L\right)^2 + \left(2\pi f L_{series}\right)^2}} - P_{series\ losses} \ \text{[W]} \quad (5)$$

2.2.2. Independent-Coil Connection

The inner stator and outer stator, each of which produces a different amount of power, are separated from the coil connection for independent coils. Equations (6) and (7) provide the electrical power generated by an IEDSG when the coil is connected independently.

$$E_{G_{inner}} = 4.44f\left(N_{inner}\right)\phi_{inner} \ \text{[V]} \quad (6)$$

$$E_{G_{outer}} = 4.44f\left(N_{outer}\right)\phi_{outer} \ \text{[V]} \quad (7)$$

where $E_{G_{inner}}$ and $E_{G_{outer}}$ represent generated rms voltages at inner and outer coils in [V]; f is the frequency of the generator in [Hz]; and ϕ_{inner} and ϕ_{outer} are the flux linkage through the inner and outer coil winding in [Wb]. The flow of the current at inner and outer coil connection is calculated using Equations (8) and (9).

$$I_{a_{inner}} = \frac{E_{G_{inner}}}{\sqrt{\left(R_{inner} + R_L\right)^2 + \left(2\pi f L_{inner}\right)^2}} \ \text{[A]} \quad (8)$$

$$I_{a_{outer}} = \frac{E_{G_{outer}}}{\sqrt{\left(R_{outer} + R_L\right)^2 + \left(2\pi f L_{outer}\right)^2}} \ \text{[A]} \quad (9)$$

where $I_{a_{inner}}$ and $I_{a_{outer}}$ represent inner and outer currents, R_{inner} and R_{outer} the inner and outer armature resistances of the coil winding, and L_{inner} and L_{outer} the inner and outer coil inductances. The total machine loss of a IEDSG is given by:

$$P_{l_{inner}} = I^2_{a_{inner}} R_{inner} + \varepsilon_h f B^a + \varepsilon_e f^2 B^2 \ \text{[W]} \quad (10)$$

$$P_{l_{outer}} = I^2_{a_{outer}} R_{outer} + \varepsilon_h f B^a + \varepsilon_e f^2 B^2 \ \text{[W]} \quad (11)$$

where $P_{l_{inner}}$ and $P_{l_{outer}}$ are the losses powers at inner and outer coils. The inner and outer output powers P_{inner} and P_{outer} generated are calculated based on Equations (12), (13), (14), and (15).

$$P_{inner} = \left(E_{G_{inner}}\right) I_{a_{inner}} - P_{inner\ losses} \ \text{[W]} \quad (12)$$

$$P_{inner} = \frac{E^2_{G_{inner}}}{\sqrt{\left(R_{inner} + R_L\right)^2 + \left(2\pi f L_{inner}\right)^2}} - P_{l_{inner}} \ \text{[W]} \quad (13)$$

$$P_{outer} = \left(E_{G_{outer}}\right) I_{a_{outer}} - P_{outer\ losses} \ \text{[W]} \quad (14)$$

$$P_{outer} = \frac{E^2_{G_{outer}}}{\sqrt{\left(R_{outer} + R_L\right)^2 + \left(2\pi f L_{outer}\right)^2}} - P_{l_{outer}} \ \text{[W]} \quad (15)$$

The total output power $P_{independent}$ combined for both inner and outer stators in a DSPM generator is

$$P_{independent} = \left(\frac{E^2_{G_{outer}}}{\sqrt{\left(R_{outer} + R_L\right)^2 + \left(2\pi f L_{outer}\right)^2}} - P_{l_{outer}}\right) + \left(\frac{E^2_{G_{inner}}}{\sqrt{\left(R_{inner} + R_L\right)^2 + \left(2\pi f L_{inner}\right)^2}} - P_{l_{inner}}\right) \ \text{[W]} \quad (16)$$

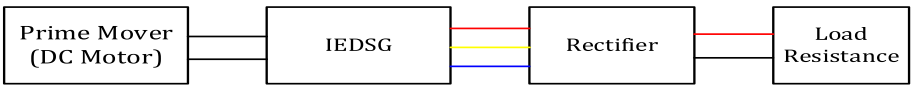

FIGURE 3. Block diagram of IEDSG analysis.

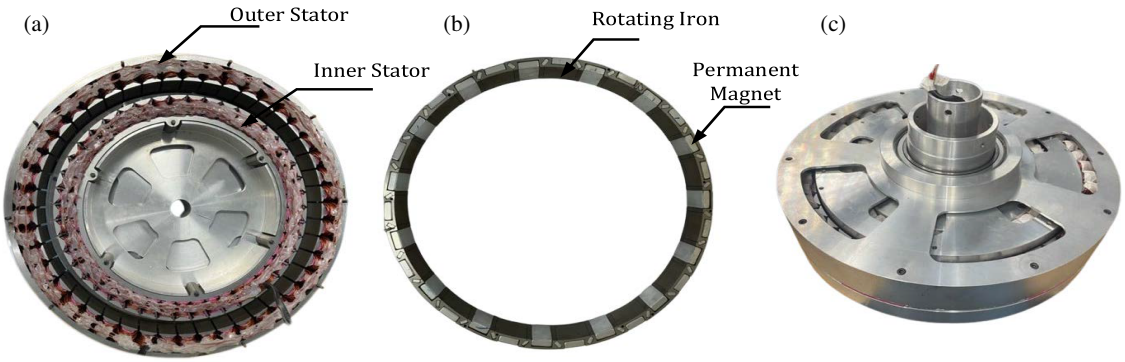

FIGURE 4. Mechanical assembly of IEDSG. (a) Inner and outer stator. (b) Permanent magnet and rotating iron. (c) Assembled IEDSG.

The amount of inductance in each coil connection will have an impact on the power produced by the proposed IEDSG based on the power equation for independent-coil and series-coil connections. The generated power is inversely proportional to the value of inductance. The maximum power generated by the proposed IEDSG will increase because of the lower inductance. Section 4 will discuss the proposed IEDSG's performance in more detail.

3. SIMULATION AND EXPERIMENTAL DESIGN

3.1. 2-D Finite Element Method

The 2D-FEM was conducted using JMAG software package developed by JSOL Corporation. Despite the apparent suitability of 3D Finite Element Method (FEM) for appropriately projecting additional IEDSG performance aspects such as magnetic flux or axial end effects, the current study was limited in scope. The analysis of these properties is outside the scope of this work due to time constraints and the computationally demanding nature of using 3D FEM. An investigation of the transient response from a simulation was carried out to forecast the IEDSG's electromagnetic properties by using Maxwell's equation [24].

$$\Omega : \frac{\partial}{\partial x}\left(v\frac{\partial y}{\partial x}\right) + \frac{\partial}{\partial y}\left(v\frac{\partial y}{\partial x}\right) = -J - v\left(\frac{\partial B_{ry}}{\partial x} - \frac{\partial B_{rx}}{\partial y}\right) + \sigma\frac{\partial A}{\partial t} \quad (17)$$

where Ω represents the field solution region of calculation; A represents the magnetic vector potential; J represents the current density; v represents the material's reluctivity; σ represents the material's electrical conductivity; B_{ry} and B_{rx} represent the remanent flux density components.

The block diagram for the proposed IEDSG's performance analysis is as shown in Figure 3. When the rotation condition of the IEDSG is set to a given speed, the rotor rotates at that speed, and a current is induced in the windings by the magnetic field produced by a permanent magnet. In a wye connection, the load resistance is linked to the rectified output of the IEDSG, converting the AC power to DC power. When evaluating the IEDSG's performance, the impacts of load resistance and IEDSG speed were considered.

3.2. Fabrication and Experimental Setup

Figure 4(a) illustrates the manufactured machine's inner and outer stators, whereas Figure 4(b) depicts the rotating iron and permanent magnet. A permanent magnet in the rotating iron is made of the material neodymium boron iron. The outer and inner stators were wound with 1 mm diameter thickness coil with 20 and 13 turns as stated in Table 2, respectively. For the stack length, the inner and outer stator rotor air gaps were kept at 3 mm and 30 mm, respectively. Figure 4(c) depicts the constructed prototype utilized for testing.

Figure 5 depicts the inner magnetic circuit and embedded permanent magnet for a double stator generator. Voltage and inductance influence the power produced by the generator, according to Lindh et al. [5]. As a result, the magnetic circuit is divided into two distinct coil connections: series-coil and independent-coil. The coils for each phase in both connections are connected in series; however, the connection of the inner and outer coils differs. The inner and outer coils are directly connected in series for the series-coil connection, but the inner and outer coils are separated for the independent-coil connection, and the total power is the sum of the outer and inner powers.

Figure 6 depicts the experimental setup used to measure the voltage, current, and power of the IEDSG. The torque sensor is connected to the primary mover, which turns the shaft of the IEDSG. When the prime mover rotates, an electric current is generated by the IEDSG's shaft, which is attached to the rotor. The rectifier is then connected to the three-phase wire,

TABLE 2. Simulation parameter.

Component	Material
Permanent Magnet	Nd-Fe-B-38H
Stators	50H800
Rotor Core	50H800
Diameter of Wire	1 mm
Number of Outer Coil Turns	20
Number of Inner Coil Turns	13
Phase Connection	wye

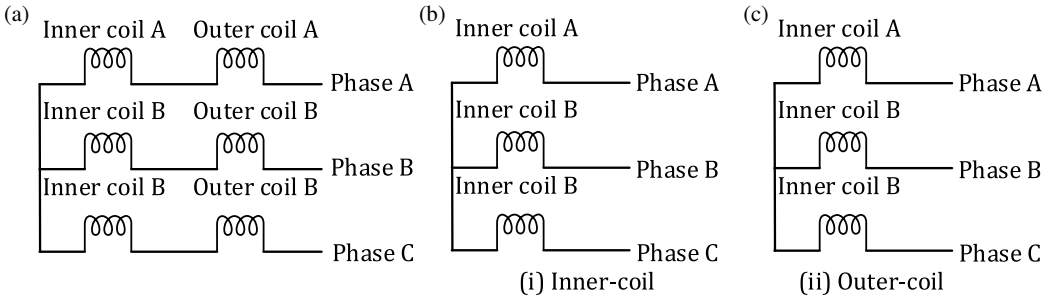

FIGURE 5. Coil-connection. (a) Series-coil. (b) Independent-coil.

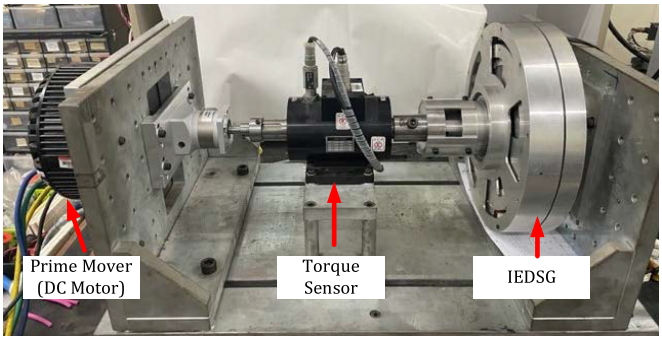

FIGURE 6. Experimental setup of IEDSG.

and the resistance is changed using an electronic programmable load. The voltage, current, and power were measured at various speeds with various resistance loads.

3.3. Validation Results

The proposed IEDSG is built and assembled based on the results of the FEM analysis to validate its functionality. Changes in load resistance of up to 50 ohms are made, and the programmable electronics load's load voltage, generated power, and load current are recorded and compared to simulation results. The load voltage and load current are the voltage drops and current through the load resistance, respectively. The dashed line in Figure 7 represents simulation data, while the solid line reflects experimental data. The graph demonstrates that the percentage variances in load voltage, load current, and generated power between simulation and experimental data are 4%, 16%, and 12%, respectively.

4. PERFORMANCE ANALYSIS

4.1. Fundamental Characteristics

Figure 8 depicts the IEDSG performance analysis for a series-coil connection with a variable load resistance up to 50 ohm and a constant speed of 800 rpm, together with the accompanying load voltage, load current, generated torque, and generated power. Figure 8(a) depicts the planned IEDSG's load voltage and load current. When the load resistance, which was inversely proportional to the load current, was reduced, so was the load voltage. The load voltage decreases due to the low cutting flux value, where the flux of the coil is greater than the flux of the permanent magnet. The load voltage and current began to saturate at a specific load resistance of 40 ohms. When the load resistance was increased beyond the peak saturation point, at a load resistance of 30 Nm at 5 ohms, the generated torque began to decrease. At a load resistance of 5 ohm, the generated power rises to 1400 W. However, for loads with resistances

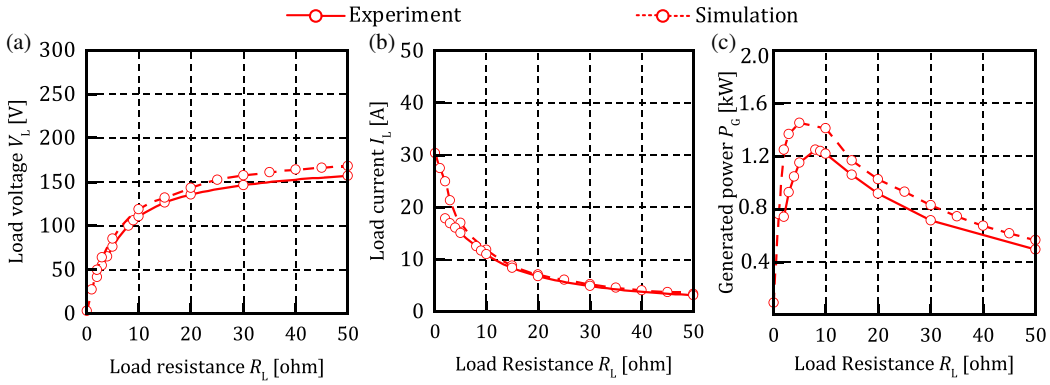

FIGURE 7. Comparison of simulation and experimental data. (a) Load voltage. (b) Load current. (c) Generated power.

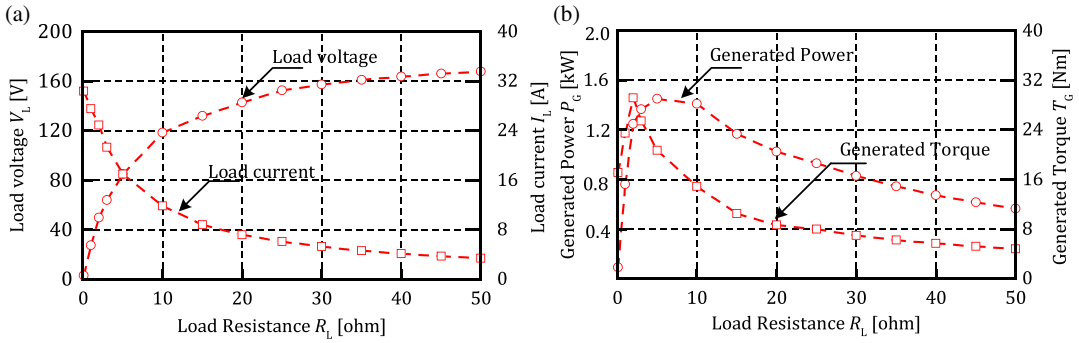

FIGURE 8. Fundamental characteristics. (a) Load voltage and load current. (b) Generated torque and generated power.

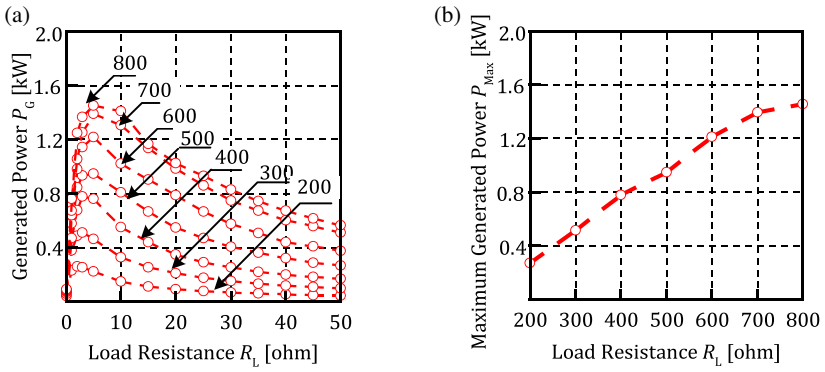

FIGURE 9. Power characteristics for different speed. (a) Characteristics of speed. (b) Maximum generated power.

greater than 5 ohms, the power output begins to decline since the current decreases as the load resistance rises.

4.2. Speed Characteristics

Figure 9 shows how the power characteristics change as the rotor speed changes. The generated power increases as the rotor speed increases due to an increase in flux flow across the air gap. The proposed IEDSG reached its power generation peak at various load resistances and speeds. For 200 RPM, the maximum power output is 270 W at 2.22 ohm of load resistance, while for 800 RPM, the maximum power output is 1455 W at 5 ohm of load resistance. It is indicated that the higher the load resistance is, the higher the power is, and the faster the rotor spins. The data is further investigated on the highest generated power for each speed, as shown in Figure 9(b). It shows how the maximum power gradually rose until the speed of 800 revolutions per minute, when it began to saturate.

4.3. Coil-Connection Characteristics

To analyze the recommended IEDSG, the performance of two distinct coil connections, including series-coil and independent-coil, was examined. The term "independent coil" is used when separating the inner and outer coils and determining the combined power of the inner and outer coils. Figure 10 depicts the power generated by connecting the inner and outer coils. Because the stator has 54% more coil turns twisted in it than the inner stator, which has 20 turns instead of 13, and the outer coil produces 54% more power.

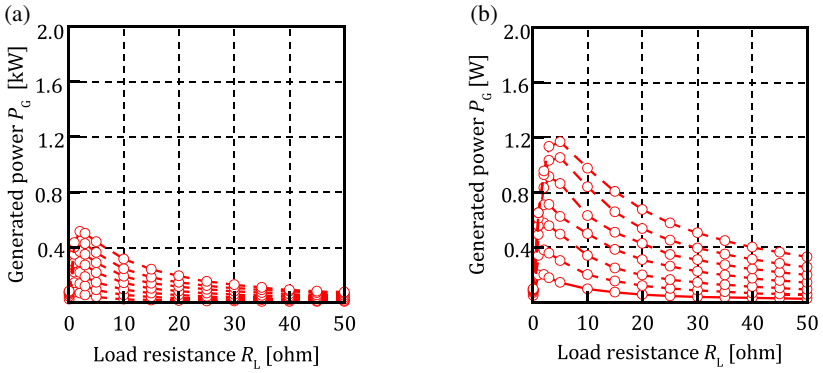

FIGURE 10. Inner-coil and outer-coil connection. (a) Inner-coil. (b) Outer-coil.

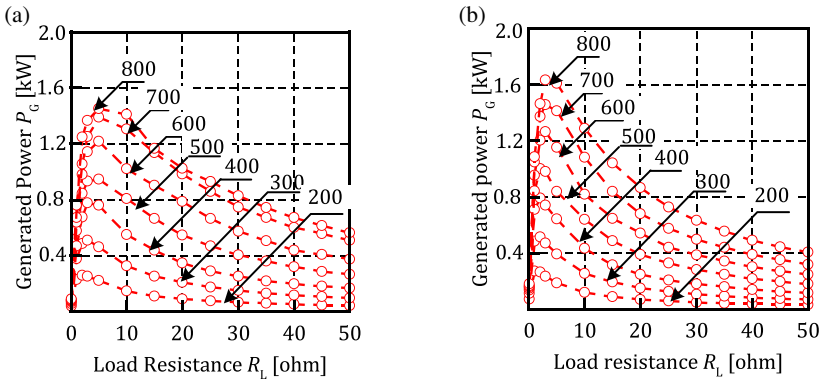

FIGURE 11. Series-coil and independent-coil connection. (a) Series-coil. (b) Independent-coil.

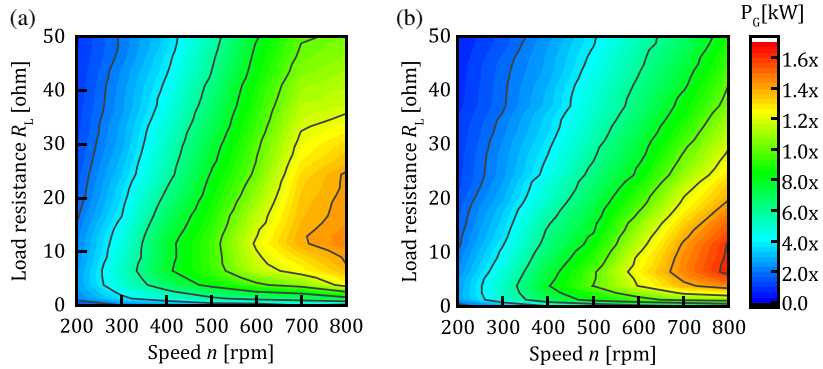

FIGURE 12. Power mapping of series-coil and independent-coil connection. (a) Series-coil. (b) Independent-coil.

When the inner-coil and outer-coil connections are compared, the outer-coil connection demonstrates the most power at all speeds. This happened because the outer-coil connection had the highest inductance value. Separating the inner and outer coils, and then adding the power provided by each coil connection can improve the proposed IEDSG's performance as shown in Figure 11. For example, at 800 rpm, the maximum power of the inner coil is 512 W while the maximum power of the outside coil is 1176 W. When the powers of the inner and outer coils are combined, the overall power generated by the proposed IEDSG is 1688 W, which is larger than the power of the series coil, which is only 1456 W, as shown in Figure 12. The independent-coil connection increases the power output of the recommended IEDSG by 16%.

The power mapping technique is used to evaluate the performance of the proposed IEDSG's coil connection. The proposed design will be utilized to change load resistance and speed. The maximum power color at 800 rpm for the series-coil connection is orangish, equating to approximately 1400 W at a load resistance of 10 ohm, whereas the maximum power color for the independent-coil connection is reddish, corresponding to 1600 W at a load resistance of 5 ohm. As a result of the power mapping, the suggested IEDSG can reach its maximum power at varying load resistances and speeds.

TABLE 3. Comparison of series-coil and independent-coil connection.

	Resistance [ohm]		Inductance [mH]		Load voltage [V]		Current [A]		Torque [Nm]	Power [W]	
	R_{C_sim}	R_{C_exp}	L_{C_exp}	L_{S_sim}	V_{L_sim}	V_{L_exp}	I_{L_sim}	I_{L_exp}	T_{G_sim}	P_{G_sim}	P_{G_exp}
Series	0.89	1.06	2.49	0.078	85	99.94	17.13	12.48	21	1456	1247
Independent	0.89	1.04	2.27	0.078	108.2	105.8	31.21	26.44	21.02	1688	1513

Table 3 compares the results for series and independent coil connections. The percentage mismatch between simulation and experimental data for series coils working at 800 rpm is 12%, while it is 9% for independent coils. The percentage difference illustrates the simulation data's dependability and acceptability. Furthermore, the coil inductance of the series coil is about 10% higher than that of the independent coils. According to the generated power equation, coil inductance affects the value of generated power, which is inversely proportional to generated power. As a result, the power generated by the series coil connection is less than that given by the independent coil connection. Independent coils outperform series coil connections in terms of effectiveness, increasing generated power by up to 16% compared to series coil connections.

5. CONCLUSIONS

In this paper, the power density and power mapping performance of a unique internal and embedded permanent magnet for a double-stator generator (IEDSG) are studied. The finite element method (FEM) is used to describe the generation capabilities, which include electromagnetic features like flux density and flux lines. The proposed IEDSG is then constructed and assembled in the lab before being tested with a load circuit. The FEM simulation produced 12% more power than the experimental data, which is both genuine and acceptable. The proposed IEDSG is used to compare the performance of two various coil connections, including series-coil and independent-coil. At 800 rpm, the maximum power generated by the independent-coil connection is 1688 W, which is 16% greater than the maximum power generated by the series-coil connection. The independent coil has a larger maximum power because the total inductance produced by the inner and outer stators is greater than that of the series coil.

REFERENCES

[1] Krause, P., O. Wasynczuk, S. D. Sudhoff, and S. Pekarek, *Analysis of Electric Machinery and Drive Systems*, 3rd ed., 121–141, IEEE Press, 2013.

[2] Lin, H., K.-Y. Hwang, and B.-I. Kwon, "An improved flux observer for sensorless permanent magnet synchronous motor drives with parameter identification," *Journal of Electrical Engineering and Technology*, Vol. 8, No. 3, 516–523, 2013.

[3] Mohammad, R. M., N. Mariun, N. Misron, M. A. M. Radzi, and S. Musa, "Broken rotor bar detection in LS-PMSM based on startup current analysis using wavelet entropy features," *Applied Sciences*, Vol. 7, No. 8, 845, 2017.

[4] Rucker, J. E., J. L. Kirtley, and T. J. McCoy, "Design and analysis of a permanent magnet generator for naval applications," in *IEEE Electric Ship Technologies Symposium*, 451–458, 2005.

[5] Lindh, T., P. Salminen, J. Pyrhonen, M. Niemela, J. Kinnunen, and J. Haataja, "Permanent magnet generator designing guidelines," in *2007 International Conference on Power Engineering, Energy and Electrical Drives*, 185–189, 2007.

[6] Gieras, J. F., R.-J. Wang, and M. J. Kamper, *Axial Flux Permanent Magnet Brushless Machines*, Kluwer Academic Publisher, London, 2004.

[7] Hendershot, J. R. and T. J. E. Miller, *Design of Brushless Permanent-Magnet Machines*, Motor Design Books, LLC, UK, 2010.

[8] Do, T. D., S. Kwak, H. H. Choi, and J.-W. Jung, "Suboptimal control scheme design for interior permanent-magnet synchronous motors: An SDRE-based approach," *IEEE Transactions on Power Electronics*, Vol. 29, No. 6, 3020–3031, 2014.

[9] Pellegrino, G., A. Vagati, P. Guglielmi, and B. Boazzo, "Performance comparison between surface-mounted and interior PM motor drives for electric vehicle application," *IEEE Transactions on Industrial Electronics*, Vol. 59, No. 2, 803–811, 2012.

[10] Yu, D., X. Y. Huang, Y. T. Fang, and J. Zhang, "Design and comparison of interior permanent magnet synchronous traction motors for high speed railway applications," in *2017 IEEE Workshop on Electrical Machines Design, Control and Diagnosis (WEMDCD)*, 58–62, Nottingham, UK, 2017.

[11] Chai, F., S. Cui, and S. Cheng, "Performance analysis of double-stator starter generator for the hybrid electric vehicle," *IEEE Transactions on Magnetics*, Vol. 41, No. 1, 484–487, Jan. 2005.

[12] Chau, K. T., Y. B. Li, J. Z. Jiang, and C. Liu, "Design and analysis of a stator-doubly-fed doubly-salient permanent-magnet machine for automotive engines," *IEEE Transactions on Magnetics*, Vol. 42, No. 10, 3470–3472, 2006.

[13] Liu, C., K. T. Chau, J. Z. Jiang, and L. Jian, "Design of a new outer-rotor permanent magnet hybrid machine for wind power generation," *IEEE Transactions on Magnetics*, Vol. 44, No. 6, 1494–1497, 2008.

[14] Norhisam, M., M. Norafiza, and C. Y. Sia, "Double stator type permanent magnet generator," in *2009 IEEE Student Conference on Research and Development (SCOReD)*, 316–319, 2009.

[15] Wang, Y., S. Niu, and W. Fu, "Electromagnetic performance analysis of novel flux-regulatable permanent magnet machines for wide constant-power speed range operation," *Energies*, Vol. 8, No. 12, 13 971–13 984, 2015.

[16] Misron, N. B., S. R. C. Ahmad, R. N. Firdaus, C. Aravind, H. Wakiwaka, and M. Nirei, "Comparative evaluation on power-speed density of portable permanent magnet generators for agricultural application," *Progress In Electromagnetics Research*, Vol. 129, 345–363, 2012.

[17] Zheng, P., Q. Wu, J. Bai, C. Tong, and Z. Song, "Analysis and experiment of a novel brushless double rotor machine for power-split hybrid electrical vehicle applications," *Energies*, Vol. 6, No. 7, 3209–3223, 2013.

[18] Vaithilingam, C. A., N. Misron, M. R. Zare, I. Aris, and M. H. Marhaban, "Computation of electromagnetic torque in a double

rotor switched reluctance motor using flux tube methods," *Energies*, Vol. 5, No. 10, 4008–4026, 2012.

[19] Liu, J., C. Gong, Z. Han, and H. Yu, "IPMSM model predictive control in flux-weakening operation using an improved algorithm," *IEEE Transactions on Industrial Electronics*, Vol. 65, No. 12, 9378–9387, 2018.

[20] Uddin, M. N. and M. M. Rahman, "Online torque-flux estimation-based nonlinear torque and flux control scheme of IPMSM drive for reduced torque ripples," *IEEE Transactions on Power Electronics*, Vol. 34, No. 1, 636–645, 2019.

[21] Norhisam, M., R. Suhairi, M. Norafiza, M. A. M. Radzi, I. Aris, M. Nirei, and H. Wakiwaka, "Comparison on performance of single phase and three phase double stator type permanent magnet generator," in *Asia-Pacific Symposium on Applied Electromagnetics and Mechanics*, 231–234, Kuala Lumpur, 2010.

[22] Norhisam, M., M. Norafiza, M. Nirei, H. Wakiwaka, M. Syafiq, and I. Aris, "Comparison on performance of a single and double stator of a slot-less permanent magnet generator," in *21st Symposium on Elctromagnetis and Dynamics*, 561–564, 2009.

[23] Song, T., Z. Zhang, H. Liu, and W. Hu, "Multi-objective optimisation design and performance comparison of permanent magnet synchronous motor for EVs based on FEA," *IET Electric Power Applications*, Vol. 13, No. 8, 1157–1166, 2019.

[24] Jian, L., K. T. Chau, and J. Z. Jiang, "A magnetic-geared outer-rotor permanent-magnet brushless machine for wind power generation," *IEEE Transactions on Industry Applications*, Vol. 45, No. 3, 954–962, 2009.